

# Manifold-Aware CycleGAN for High Resolution Structural-to-DTI Synthesis

Benoit Anctil-Robitaille , Christian Desrosiers, Herve Lombaert

ETS Montreal, Canada

**Abstract.** Unpaired image-to-image translation has been applied successfully to natural images but has received very little attention for manifold-valued data such as in diffusion tensor imaging (DTI). The non-Euclidean nature of DTI prevents current generative adversarial networks (GANs) from generating plausible images and has mostly limited their application to diffusion MRI scalar maps, such as fractional anisotropy (FA) or mean diffusivity (MD). Even if these scalar maps are clinically useful, they mostly ignore fiber orientations and have, therefore, limited applications for analyzing brain fibers, for instance, impairing fiber tractography. Here, we propose a manifold-aware CycleGAN that learns the generation of high resolution DTI from unpaired T1w images. We formulate the objective as a Wasserstein distance minimization problem of data distributions on a Riemannian manifold of symmetric positive definite  $3 \times 3$  matrices  $\text{SPD}(3)$ , using adversarial and cycle-consistency losses. To ensure that the generated diffusion tensors lie on the  $\text{SPD}(3)$  manifold, we exploit the theoretical properties of the exponential and logarithm maps. We demonstrate that, unlike standard GANs, our method is able to generate realistic high resolution DTI that can be used to compute diffusion-based metrics and run fiber tractography algorithms. To evaluate our model's performance, we compute the cosine similarity between the generated tensors principal orientation and their ground truth orientation and the mean squared error (MSE) of their derived FA values. We demonstrate that our method produces up to 8 times better FA MSE than a standard CycleGAN and 30% better cosine similarity than a manifold-aware Wasserstein GAN while synthesizing sharp high resolution DTI.

## 1 Introduction

Unpaired image-to-image translation and image synthesis have been widely used in medical imaging [15]. Whether they are employed to generate missing modalities, normalize images or enhance images quality and resolution, generative adversarial networks (GANs) [5] have been proven effective in multiple challenging medical image analysis tasks. However, they have been mainly studied on real-valued images, thus impeding the development of applications for manifold-valued data such as diffusion tensor images (DTI). Despite the growing interest in the brain's structural connectivity, applications of GANs to DTI have been mostly limited to generating derived scalar maps like fractional anisotropy (FA)

and mean diffusivity (MD), which ignore the fibers’ orientation and provide limited insights on their structural organization.

Among the literature, [6] investigates the generation of diffusion MRI scalar maps from T1w images using a CycleGAN [17]. The authors show that the structural and diffusion spaces share a sufficient amount of information to be able to synthesize realistic FA and MD maps from downsampled T1w images. In [16], dual GANs and Markovian discriminators are used to harmonize multi-site FA and MD maps of neonatal brains. They demonstrate that using a GAN-like architecture can better capture the complex non-linear relations between multiple domains than standard normalization methods.

While the previously mentioned works manifest applications of GANs on DTI-derived metrics, they do not tackle the challenge of generating DTI. Being able to synthesize such images would unlock a vast amount of useful methods that are already well studied on real-valued modalities, while preserving all the geometrical information encoded in the diffusion tensors. However, DTI data is manifold-valued where the data of each voxel lies on a Riemannian manifold of symmetric positive definite  $3 \times 3$  matrices, i.e., the SPD(3) manifold. The non-Euclidean nature of DTI prevents standard GANs from generating plausible images as there is no guarantee that the generated diffusion tensors lie on the SPD(3) manifold. One solution, presented in [2], is to employ the Log-Euclidean metric to accurately process data on the SPD(n) manifold. By using the log and exp projections proposed in [2], one can apply Euclidean operations on tensors and guarantee that the resulting tensors will lie on such manifold. Those computationally efficient mapping operations form an interesting framework for manifold-valued data learning and have been used in [8] to develop a deep neural network that learns discriminative SPD matrices called SPDNet. With the help of the matrix backpropagation of spectral layers defined in [10], they designed a network that learns data on SPD(n). Nonetheless, SPDNet [8] is limited to single SPD matrix learning and cannot help in learning multiple spatially organized SPD matrices as it is the case with DTI.

Related to our work, [9] proposes a manifold-aware Wasserstein GAN for manifold-valued data generation that leverages the aforementioned log and exp mappings. In their work, they generate plausible slices of DTI from noise vectors. By comparing the produced images of their network with those produced by a regular Wasserstein GAN, one can clearly see that the manifold mappings are necessary to produce credible diffusion tensors. However, the proposed manifold-aware Wasserstein GAN could not provide any additional clinical insights, nor help in understanding the brain’s connectivity as the generated images are not conditioned by any real contextual information such as T1w images. Furthermore, [9] only focus on the generation of 2D DTIs which is of limited application for the assessment of the structural organization of the brain’s fibers.

This paper presents a novel manifold-aware CycleGAN that generates high resolution (HR) DTI from unpaired T1w images. Our method leverages the detailed structural information provided by T1w images while constraining the syn-

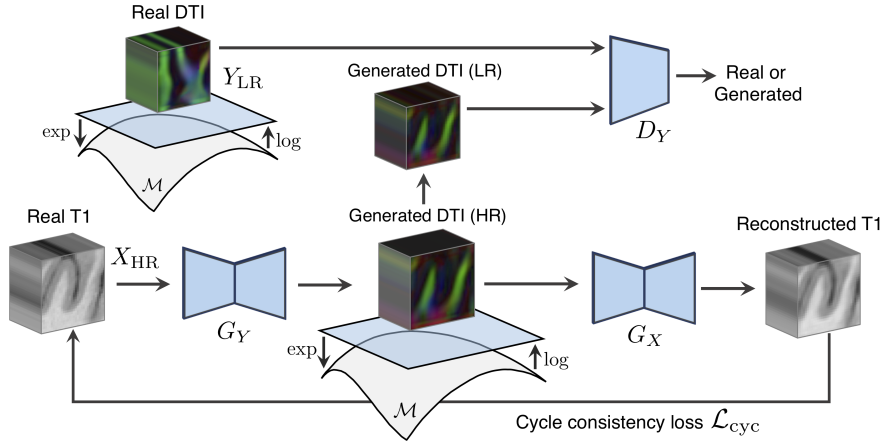


**Fig. 1.** The forward cycle of our manifold-aware CycleGAN.  $G_Y$  generates high resolution DTIs on the SPD(3) manifold using the  $\log_{\text{Id}}$  and  $\exp_{\text{Id}}$  mapping.  $D_Y$  assesses the generated images quality and provides feedback to  $G_Y$ .  $G_X$  tries to reconstruct the original T1w images from  $\log_{\text{Id}}(\exp_{\text{Id}}(G_Y(\mathbf{x})))$ .

thesized diffusion tensors to lie on the SPD(3) manifold using the Log-Euclidean metric. Specifically, the contributions of this work are as follows:

- We present the first CycleGAN model for the unpaired mapping between images and SPD(3) manifold-valued data.
- This is also the first deep learning model to generate DTI data from structural MRI. As mentioned before, previous approaches have focused on generating diffusion scalar maps like FA or MD, and not diffusion tensors as in this work.

Our proposed manifold-aware GycleGAN method is presented in the next section.

## 2 Method

Let  $X_{\text{HR}}$  be the domain of high resolution structural images and  $Y_{\text{HR}}$  be the domain of high resolution diffusion tensor images. Our goal is to learn mapping functions  $G_Y : X_{\text{HR}} \mapsto Y_{\text{HR}}$  and  $G_X : Y_{\text{HR}} \mapsto X_{\text{HR}}$  that translate the real-valued domain  $X_{\text{HR}}$  into the manifold-valued domain  $Y_{\text{HR}}$  and the other way around. However, as it is often the case, we do not have access to high resolution DTI. Thus, we train our model with unpaired training samples  $\{\mathbf{x}_i\}_{i=1}^N$  where  $\mathbf{x}_i \in X_{\text{HR}}$  is a 3D structural image (e.g., T1w), and  $\{\mathbf{y}_j\}_{j=1}^M$  where  $y_j \in Y_{\text{LR}}$  is a DT image with lower resolution. We employ the  $\log_{\text{Id}}$  and  $\exp_{\text{Id}}$  mapping to project the generated and the real DTI on the tangent plane at the  $3 \times 3$  identity matrix to ensure that  $G_Y(\mathbf{x})$  lie on the SPD(3) manifold and to compare

the manifold-valued data distributions as in [9]. Two discriminators,  $D_X$  and  $D_Y$ , assess the quality of the generated images  $G_X(\mathbf{y})$  and generated downsampled DTI  $\downarrow \log_{\text{Id}}(\exp_{\text{Id}}(G_Y(\mathbf{x})))$  with respect to their real data distributions  $G_X(\mathbf{y}) \sim \mathbb{P}_{X_{HR}}$  and  $\downarrow \log_{\text{Id}}(\exp_{\text{Id}}(G_Y(\mathbf{x}))) \sim \mathbb{P}_{\log_{\text{Id}}(Y_{LR})}$ . We formulate the objective as a Wasserstein distance minimization problem on the SPD(3) manifold with an adversarial and a cycle-consistent loss. The adversarial portion of the objective helps the generators  $G_X$  and  $G_Y$  to generate images that match the target distribution. On the other hand, the cycle-consistent losses provide high resolution gradients that are necessary to generate high resolution DTI with a proper structure.

## 2.1 Log-Euclidean Metric

Diffusion tensor matrices are well defined in the Log-Euclidean metric, where a matrix logarithm and exponential can be conveniently processed in one metric and always be mapped back to valid symmetric diffusion tensors [2]. Let  $\mathbf{M} = \mathbf{U}\mathbf{\Sigma}\mathbf{U}^\top$  be the eigen-decomposition of a symmetric matrix  $\mathbf{M}$ . The computation of the logarithm and the exponential of a tensor noted as  $\log_{\text{Id}}$  and  $\exp_{\text{Id}}$  are defined as follows:

$$\forall \mathbf{P} \in S_*^+, \log_{\text{Id}}(\mathbf{P}) = \mathbf{U} \log(\mathbf{\Sigma}) \mathbf{U}^\top \in \mathcal{T}_{\text{Id}} \quad (1)$$

$$\forall \mathbf{S} \in \mathcal{T}_{\text{Id}}, \exp_{\text{Id}}(\mathbf{S}) = \mathbf{U} \exp(\mathbf{\Sigma}) \mathbf{U}^\top \in S_*^+ \quad (2)$$

We use these maps throughout our work to project the generated and real DTI on the SPD(3) manifold and on the tangent plane at the  $3 \times 3$  identity matrix  $\mathcal{T}_{\text{Id}}$ .

## 2.2 Adversarial Loss

In a traditional GAN setup [5], a generator  $G$  and a discriminator  $D$  compete in a minimax game where  $G$  tries to generate data so close to a true data distribution that  $D$  cannot identify if the generated data is real or not. In [1],  $D$  is replaced by a discriminator that leverages the Wasserstein distance to estimate how close to the real data distribution the generated one is. The Wasserstein GAN (WGAN) architecture tends to stabilize the training as the Wasserstein distance never saturates, thus always provides relevant gradients to  $G$ . The adversarial part of our objective follows the WGAN framework and is defined as follows:

$$\begin{aligned} \mathcal{L}_{\text{WGAN}}(G_Y, D_Y, X_{HR}, Y_{LR}) &= \mathbb{E}_{\mathbf{y} \sim \mathbb{P}_{Y_{LR}}} [D_Y(\log_{\text{Id}}(\mathbf{y}))] \\ &- \mathbb{E}_{\mathbf{x} \sim \mathbb{P}_{X_{HR}}} [D_Y(\downarrow \log_{\text{Id}}(\exp_{\text{Id}}(G_Y(\mathbf{x}))))] \end{aligned} \quad (3)$$

For simplicity, we only show the DTI related part of the adversarial loss in 3. In our case,  $G_Y$  generates high resolution DTIs that are projected on the SPD(3) manifold using the exp and log mapping as in [9]. Since we only have real samples from the low-resolution data distribution  $\mathbf{y} \sim \mathbb{P}_{Y_{LR}}$ , the generated images are downsampled using trilinear interpolation prior to the discriminator

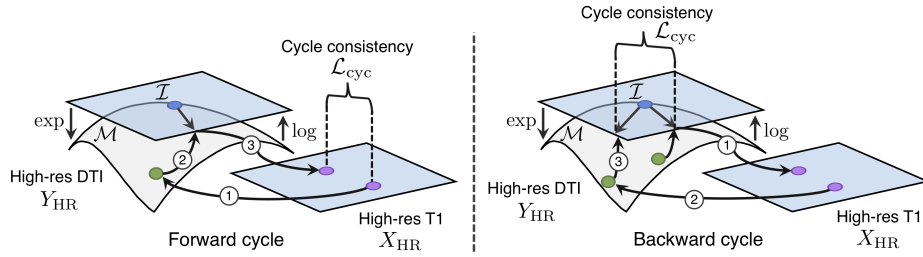


**Fig. 2.** On the left, our forward cycle: A T1w image is translated to a high resolution DTI on the SPD(3) manifold and back to the T1w domain where the cycle consistent loss is computed. On the right, our backward cycle: An upsampled DTI on  $\mathcal{T}_{\text{Id}}$  is translated to the T1w domain and back to  $\mathcal{T}_{\text{Id}}$  where the cycle consistent loss is computed

assessment.  $D_Y$  measures the Wasserstein distance between the data distribution of downsampled generated images and the data distribution of real low-resolution DTI using the Log-Euclidean metric [2].

### 2.3 Cycle Consistency Loss

The adversarial loss alone is not sufficient to drive the generation of high resolution DTIs. Because the discriminator  $D_Y$  only assesses downsampled images so its feedback cannot help  $G_Y$  improving beyond a certain level of detail. To mitigate this problem, we introduce a cycle consistency loss [17] that enforces the forward and backward cycle consistency of the network. In our case, the forward cycle consistency ensures that from the translated DTI  $\log_{\text{Id}}(\exp_{\text{Id}}(G_Y(\mathbf{x})))$  we are able to reconstruct the corresponding original structural images  $\mathbf{x} \sim \mathbb{P}_{X_{\text{HR}}}$  that are originally in high resolution. The backward cycle consistency ensures that from the translated structural images  $G_X(\uparrow \log_{\text{Id}}(\mathbf{y}))$  we are able to reconstruct the original upsampled DTI  $\mathbf{y} \sim \mathbb{P}_{\log_{\text{Id}}(Y_{\text{LR}})}$ . Our full cycle consistency loss is defined as:

$$\begin{aligned} \mathcal{L}_{\text{cyc}}(G_Y, G_X) = & \mathbb{E}_{\mathbf{x} \sim \mathbb{P}_{X_{\text{HR}}}} [\|G_X(\log_{\text{Id}}(\exp_{\text{Id}}(G_Y(\mathbf{x})))) - \mathbf{x}\|_1] \\ & + \mathbb{E}_{\mathbf{y} \sim \mathbb{P}_{Y_{\text{LR}}}} [\|\log_{\text{Id}}(\exp_{\text{Id}}(G_Y(G_X(\uparrow \log_{\text{Id}}(\mathbf{y})))) - \uparrow \log_{\text{Id}}(\mathbf{y})\|_1] \end{aligned} \quad (4)$$

### 2.4 Manifold-Aware Wasserstein CycleGAN

Our full objective is:

$$\begin{aligned} \mathcal{L}(G_X, G_Y, D_X, D_Y) = & \mathcal{L}_{\text{WGAN}}(G_X, D_X, Y_{\text{LR}}, X_{\text{HR}}) \\ & + \mathcal{L}_{\text{WGAN}}(G_Y, D_Y, X_{\text{HR}}, Y_{\text{LR}}) + \mathcal{L}_{\text{cyc}}(G_Y, G_X) \end{aligned} \quad (5)$$

The adversarial parts  $\mathcal{L}_{\text{WGAN}}(G_X, D_X, Y_{\text{LR}}, X_{\text{HR}})$  and  $\mathcal{L}_{\text{WGAN}}(G_Y, D_Y, X_{\text{HR}}, Y_{\text{LR}})$  of our full objective guide the generators  $G_X$  and  $G_Y$  towards the synthesis of

images close to their real data distributions using a Wasserstein distance on the SPD(3) manifold. The cycle consistency denoted as  $\mathcal{L}_{\text{cyc}}(G_Y, G_X)$  gives fine-grained retro-action that helps generate HR DTI while preventing mode collapse.

### 3 Experiments

**Data** We employ the pre-processed T1-weighted (T1w) and diffusion MRI (dMRI) data of 1065 patients from the HCP1200 release of the Human Connectome Project [14] to evaluate our manifold-aware CycleGAN. The T1w (0.7 mm isotropic, FOV = 224mm, matrix = 320, 256 sagittal slices in a single slab) and diffusion (sequence = Spin-echo EPI, repetition time (TR) = 5520 ms, echo time (TE) = 89.5ms, resolution =  $1.25 \times 1.25 \times 1.25$  mm<sup>3</sup> voxels) data acquisition was done using a Siemens Skyra 3T scanner [13] and pre-processed following [4]. The diffusion tensors were fitted using DSI Studio toolbox [11]. Both T1w and DTI were decomposed in overlapping patches of  $32^3$  voxels centered on the foreground with stride of  $8^3$  voxels.

**Experiments Setup** We used 25 000 unpaired T1w and DTI patches randomly selected among 250 subjects as our training set. For the evaluation set and test set, 5000 and 3000 paired T1w and DTI patches were randomly selected among 10 subjects. We compared our method with two baselines: a manifold-aware Wasserstein GAN and a CycleGAN without the  $\log_{\text{Id}}$  and  $\exp_{\text{Id}}$  mappings. These baseline methods allow us to assess the impact of both the cycle consistency and the manifold mapping. We measure the quality of the generated HR DTI by computing two metrics: a) the mean cosine similarity between the principal eigen-vectors of the generated images and their ground truth and b) the mean squared error between the FA of the generated images and their ground truth. While the cosine similarity allows us to evaluate the precision of the predicted orientation of the generated tensors, the mean squared error on the derived FA highlights the network’s ability to estimate local diffusion restriction. Furthermore, a qualitative inspection of the generated DTI is performed.

**Implementation Details** Both generators are based on the 3D-Unet implementation from [3] with slightly different last layers to fit the scale of the generated data. For  $G_X$ , we use a sigmoid as the final activation function to generate values in the range [0,1]. For  $G_Y$  we use a hard hyperbolic tangent activation function followed by the  $\exp_{\text{Id}}$  and  $\log_{\text{Id}}$  projection to generate diffusion tensors on the SPD(3) manifold. Furthermore, we apply a symmetry constraint on the 9-channels output of  $G_Y$  using  $\frac{1}{2}(\mathbf{X} + \mathbf{X}^\top)$ . For our discriminators, we use a Resnet-18 architecture [7] where all convolutions have been changed to 3D convolutions. Both the generators and the discriminators were trained with the Adam optimizer [12] and a batch size of 8 for 20 epochs. A starting learning rate of  $1 \times 10^{-4}$  was used jointly with a reduce on plateau strategy. To stabilize the training of our network, we pre-trained the generators independently with 25 000 paired patches randomly sampled from 10 subjects during 10 epochs.

**Table 1.** FA MSE and cosine similarity of compared methods. Note: a smaller FA MSE corresponds to a superior performance while a higher cosine similarity is better.

Models	FA MSE	Cosine Similarity
Manifold-Aware WGAN	0.0368	0.4512
CycleGAN	0.0931	0.5371
<b>Manifold-Aware CycleGAN (Ours)</b>	<b>0.0113</b>	<b>0.5846</b>

**Fibers Orientation Analysis** To evaluate the predicted tensor orientation, we compute the cosine similarity between the principal orientation of each generated tensor and its ground truth. Results in Table 1 demonstrate that our method perform better than the two baselines with an average cosine similarity of 0.5846 compared to 0.4512 for the manifold-aware WGAN and 0.5371 for the CycleGAN without manifold mapping. Our method is able to better estimate the orientation of the fibers which is an essential information for most tractography algorithms.

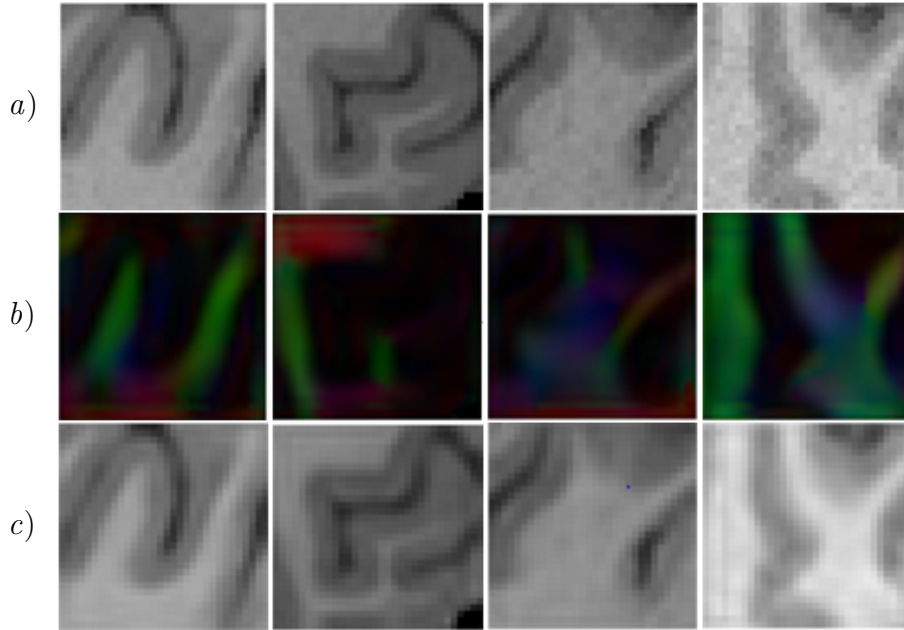


**Fig. 3.** a) Real high resolution T1 images, b) generated high resolution DTI and c) recovered T1 images (best viewed in color)

**FA Analysis** In addition to the fibers' principal orientation, we evaluate the generated HR DTI FA. FA is one of the most commonly used DT derived metrics,

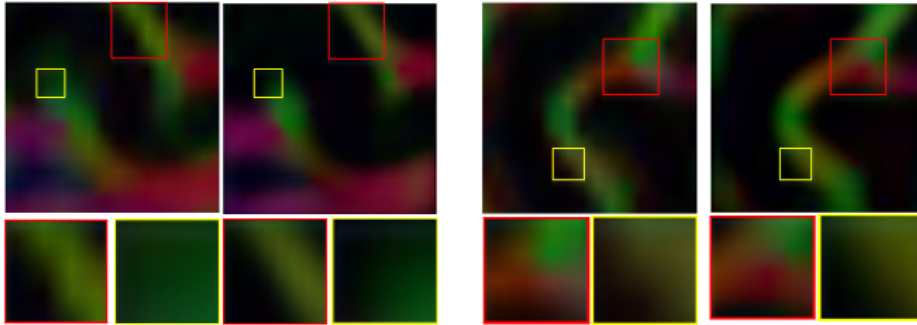


**Fig. 4.** Comparisons of two generated HR DTI and their corresponding interpolated ground truth using trilinear interpolation. One can clearly see that the generated HR DTI is sharper and contains less interpolation artifacts than its interpolated counterparts.

thus being able to generate good FA values from the generated DTI is critical. Table 1 shows the different mean squared error values for our method and the two baselines. Our manifold-aware CycleGAN performs much better than the manifold-aware WGAN and the standard CycleGAN with an MSE of 0.0113 compared to 0.0368 and 0.0931. Furthermore, we observe that the two methods using manifold mapping perform better than the standard CycleGAN. This performance gap is due to the fact that without projecting the generated data on the  $SPD(3)$  manifold using the Log-Euclidean metric, there is no guarantee that the generated tensors lie on such manifold. Consequently, the tensors eigenvalues used in the computation of FA are not strictly positive which increase the differences between the generated FA and the ground truth.

## 4 Conclusion

In this paper we proposed a novel manifold-aware CycleGAN that successfully leverages the Log-Euclidean metric and the structural information of T1w images to generate realistic high resolution DTI. Our method outperformed the manifold-aware GAN and the standard CycleGAN architecture in terms of tensor orientation estimation and MSE of derived FA. These results not only confirm that projecting the generated DTI on the  $SPD(3)$  manifold helps producing plausible diffusion tensors but also that the extra structural information provided by the T1w data is necessary to synthesize high resolution DTI. We believe that our method is an important contribution to medical image computing as it unlocks a vast number of applications on manifold-valued data.



## 5 Acknowledgments

This work was supported financially by the Research Council of Canada (NSERC), the Fonds de Recherche du Quebec (FQRNT), ETS Montreal, and NVIDIA with the donation of a GPU.

## References

1. Arjovsky, M., Chintala, S., Bottou, L.: Wasserstein GAN (2017)
2. Arsigny, V., Fillard, P., Pennec, X., Ayache, N.: Log-Euclidean metrics for fast and simple calculus on diffusion tensors. *Magnetic Resonance in Medicine* (2006)
3. Çiçek, Ö., Abdulkadir, A., Lienkamp, S.S., Brox, T., Ronneberger, O.: 3D U-Net: Learning Dense Volumetric Segmentation from Sparse Annotation. *Lecture Notes in Computer Science (including subseries Lecture Notes in Artificial Intelligence and Lecture Notes in Bioinformatics)* (2016)
4. Glasser, M.F., Sotiropoulos, S.N., Wilson, J.A., Coalson, T.S., Fischl, B., Andersson, J.L., Xu, J., Jbabdi, S., Webster, M., Polimeni, J.R., Van Essen, D.C., Jenkinson, M.: The minimal preprocessing pipelines for the Human Connectome Project. *NeuroImage* (2013)
5. Goodfellow, I.J., Pouget-Abadie, J., Mirza, M., Xu, B., Warde-Farley, D., Ozair, S., Courville, A., Bengio, Y.: Generative adversarial nets. In: *Advances in Neural Information Processing Systems*. Neural information processing systems foundation (2014)
6. Gu, X., Knutsson, H., Nilsson, M., Eklund, A.: Generating Diffusion MRI Scalar Maps from T1 Weighted Images Using Generative Adversarial Networks. *Tech. rep.* (2019)
7. He, K., Zhang, X., Ren, S., Sun, J.: Deep residual learning for image recognition. In: *Proceedings of the IEEE Computer Society Conference on Computer Vision and Pattern Recognition*. IEEE Computer Society (2016)
8. Huang, Z., Van Gool, L.: A riemannian network for SPD matrix learning. *31st AAAI Conference on Artificial Intelligence, AAAI 2017* (2017)
9. Huang, Z., Wu, J., Van Gool, L.: Manifold-Valued Image Generation with Wasserstein Generative Adversarial Nets. *Proceedings of the AAAI Conference on Artificial Intelligence* pp. 3886–3893 (2019)
10. Ionescu, C., Vantzos, O., Sminchisescu, C.: Matrix backpropagation for deep networks with structured layers. *Tech. rep.* (2015)
11. Jiang, H., Van Zijl, P.C.M., Kim, J., Pearlson, G.D., Mori, S.: DtiStudio: Resource program for diffusion tensor computation and fiber bundle tracking (2005)
12. Kingma, D.P., Ba, J.L.: Adam: A method for stochastic optimization. In: *3rd International Conference on Learning Representations, ICLR 2015 - Conference Track Proceedings*. International Conference on Learning Representations, ICLR (2015)
13. Sotiropoulos, S.N., Jbabdi, S., Xu, J., Andersson, J.L., Moeller, S., Auerbach, E.J., Glasser, M.F., Hernandez, M., Sapiro, G., Jenkinson, M., Feinberg, D.A., Yacoub, E., Lenglet, C., Van Essen, D.C., Ugurbil, K., Behrens, T.E.: Advances in diffusion MRI acquisition and processing in the Human Connectome Project. *NeuroImage* (2013)
14. Van Essen, D.C., Smith, S.M., Barch, D.M., Behrens, T.E., Yacoub, E., Ugurbil, K.: The WU-Minn Human Connectome Project: An overview. *NeuroImage* (2013)

15. Yi, X., Walia, E., Babyn, P.: Generative adversarial network in medical imaging: A review. *Medical Image Analysis* **58** (2019)
16. Zhong, J., Wang, Y., Li, J., Xue, X., Liu, S., Wang, M., Gao, X., Wang, Q., Yang, J., Li, X.: Inter-site harmonization based on dual generative adversarial networks for diffusion tensor imaging: Application to neonatal white matter development. *BioMedical Engineering Online* **19** (2020)
17. Zhu, J.Y., Park, T., Isola, P., Efros, A.A.: Unpaired Image-to-Image Translation Using Cycle-Consistent Adversarial Networks. *Proceedings of the IEEE International Conference on Computer Vision* (2017)